Fitoterapia 169 (2023) 105622

Contents lists available at ScienceDirect

Fitoterapia

journal homepage: www.elsevier.com/locate/fitote

Antinociceptive effect of cyclic and linear diterpenoids as new atypical agonists of κ-opioid receptors obtained from four species of the *Baccharis* genus, and vehiculated in nanometric niosomes

Matías Funes [a,b,*], Rodrigo D. Tosso [b], Noelia D. Machado [c,d], Mariana A. Fernández [c,e], María Garro [a], David Díaz Díaz [f,g,h], Virginia Juan Hikawczuk [i], Ricardo D. Enriz [a,b,*]

[a] Pharmacognosy, School of Chemistry, Biochemistry, and Pharmacy, National University of San Luis, Av. Ejército de los Andes 950, 5700 San Luis, Argentina
[b] Multidisciplinary Institute for Biological Research (IMIBIO-CONICET), Av. Ejército de los Andes 950, 5700 San Luis, Argentina
[c] Departamento de Química Orgánica, Facultad de Ciencias Químicas, Universidad Nacional de Córdoba, Ciudad Universitaria, Córdoba X5000HUA, Argentina
[d] Instituto de Investigación y Desarrollo en Ingeniería de Procesos y Química Aplicada (IPQA-UNC-CONICET), Avda. Vélez Sársfield 1611, Córdoba X5016GCA, Argentina
[e] Instituto de Investigaciones en Físico-Química de Córdoba (INFIQC-CONICET), Ciudad Universitaria, Córdoba X5000HUA, Argentina
[f] Departamento de Química Orgánica, Universidad de la Laguna, La Laguna, Spain
[g] Instituto Universitario de Bio-Orgánica Antonio González, Universidad de la Laguna, La Laguna, Spain
[h] Institute of Organic Chemistry, University of Regensburg, Universitätstr. 31, Regensburg 93053, Germany
[i] Organic Chemistry, School of Chemistry, Biochemistry, and Pharmacy, National University of San Luis, Av. Ejército de los Andes 950, 5700, San Luis, Argentina

ARTICLE INFO

Keywords:
Baccharis
Neoclerodane
Antinociceptive
KOR
Niosomes

ABSTRACT

New natural analgesic compounds that act in KORs are important alternatives for potential therapeutical use in medicine. In this work, we report and compare here the antinociceptive activity displayed by cyclic and linear diterpenes, obtained from the genus *Baccharis*. The antinociceptive activities determined were relatively strong, in comparison whit morphine. The antinociceptive mechanism of action was made through naloxone administration (a non-selective antagonist of opioid receptors). The more active compounds were vehiculized successfully in niosomes at nanometric scale. The observed antinociceptive activity for Bartemidiolide oxide (**BARTO**), obtain from *Baccharis artemisioides*, was greater than Flabeloic acid dimer (**DACD**), the first compound isolated from *Baccharis flabellata* that was reported possessing antinociceptive effects. We also conducted docking calculations and molecular dynamics simulations, which suggested that the newly identified diterpenes might share the molecular action mechanism reported for Salvinorin A (**SalA**). Molecular simulations have allowed us to appreciate some subtle differences between molecular interactions of these ligands stabilizing their respective complexes; such information might be useful for designing and searching for new inhibitors of KORs.

1. Introduction

Global Pain Drugs Market reached $78.41 billion in 2022, however, it is expected to reach >115.5 billion by 2032 [1]. The management of pain encompasses a variety of physiological mechanisms, such as targeting the nociceptors. Based on drug classes, the market is categorized

Abbreviations: AMSL, Above mean sea level; *i.p.*, Administered via the intraperitoneal route; *s.c.*, Administered via the subcutaneous; ANMAT, Administración Nacional de Medicamentos, Alimentos y Tecnología Médica; CNS, Central nervous system; CTLC, Centrifugal thin layer chromatography; MD, Molecular Dynamics; NSAID, Nonsteroidal anti-inflammatory drugs; SalA, Salvinorin A; SAR, Structure-Activity Relationship; KOR, κ-opioid receptor; MOR, μ-opioid receptor; DOR, δ-opioid receptor; **DAC**, ent-15,16-epoxy-19-hydroxy-1,3,13(16),14-clerodatetraen-18-oic acid; **DACD**, (1R,4S,4aS,4bR,5S,6R,8aS,10aR)-3-(2-((1S,2R,4aS,8aR)-5-carboxy-4a-(hydroxymethyl)-1,2-dimethyl-1,2,3,4,4a,8a-hexahydronaphthalen-1-yl)ethyl)-5-(2-(furan-3-yl)ethyl)-8a-(hydroxymethyl)-5,6-dimethyl-1,4,4a,4b,5,6,7,8,8a,10a-decahedron-1,4-epoxyphenanthrene-9-carboxylic acid; **BARTO**, 5′-(furan-3-yl)-4,11-dimethylspiro[10,13-dioxatetracyclo[6.3.2.01,6.09,11]tridecane-5,3′-oxolane]-2′,12- dione; **HAW**, (4aR,5S,6R,8aS)-5-[2-(furan-3-yl)ethyl]-8a-(hydroxymethyl)-5,6-dimethyl-3,4,4a,6,7,8-hexahydronaphthalene-1-carboxylic acid; **THYM**, (2Z,6Z)-6-(3-(furan-3-yl)propylidene)-2-(4-methylpent-3-en-1-yl)hept-2-enedioic acid.

* Corresponding authors at: Instituto Multidisciplinario de Investigaciones Biológicas (IMIBIO-CONICET), Universidad Nacional de San Luis, Chacabuco 915, 5700 San Luis, Argentina.
E-mail addresses: matiasdfunes@gmail.com (M. Funes), denriz@unsl.edu.ar (R.D. Enriz).

https://doi.org/10.1016/j.fitote.2023.105622
Received 10 April 2023; Received in revised form 24 July 2023; Accepted 24 July 2023
Available online 29 July 2023

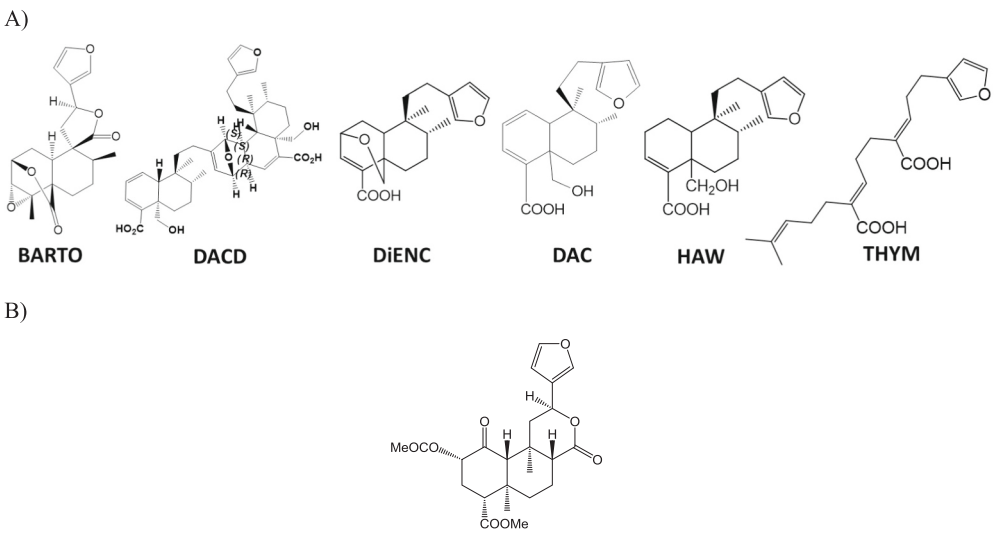

Fig. 1. A) neoclerodane diterpene compounds of different *Baccharis* genus. B) First natural whit high antinociceptive effect, specific for KOR.

into nonsteroidal anti-inflammatory drugs (NSAIDs), anesthetics, anticonvulsants, antimigraine agents, antidepressants, opioids, and nonnarcotic analgesics. Opioids are further classified into tramadol, hydrocodone, oxycodone, and others (opioids include fentanyl, morphine, meperidine, codeine, and methadone). Opioids in the treatment of chronic pain are also influenced by the fact that these potent analgesics are associated with a significant number of side effects and complications. Common side effects of opioid administration include sedation, dizziness, nausea, vomiting, constipation, physical dependence, tolerance, and respiratory depression [2].

Opioid medications that mimic endogenous opioid peptides (dynorphins, endorphins, and enkephalins) typically bind to subtypes of opioid receptors (KOR, MOR, and/or DOR) to suppress pain [3]. The KOR ligands are important research tools and promising molecules for the safer treatment of pain [4]. To address this issue, medicinal chemistry provided different approaches. The pioneering tactic consisted of synthesizing selective KOR and DOR agonists to overcome the adverse effects of MOR agonists [5].

In 2002, opioid receptors were implicated in the actions of the psychoactive mint *Salvia divinorum*. The main active constituent isolated from the leaves of *S. divinorum* is the neoclerodane diterpene **SalA** (Fig. 1A) [6]. This molecule is interesting to pharmacologists because it is a non-serotonergic hallucinogen that lacks basic nitrogen and is a potent and selective agonist for KOR. Synthetic organic chemists also found it an attractive target because of its unique structure containing seven chiral centers and a diterpene scaffold. Opioid agonists based on **SalA** have the potential to treat pain, cough, diarrhea, stimulant dependence, and mood disorders [7]. Thus, antagonists derived from this compound have potential use in treating several medical conditions, including drug dependence, depression, opioid-induced constipation, and obesity. From such characteristics, analogs of **SalA** may prove to be excellent research tools and provide greater insight into opioid receptor-mediated phenomena.

Previously, researchers at the University of San Luis reported several clerodanes and neoclerodanes obtained from *Baccharis* (Asteraceae, Astereae) genus possessing different biological effects [8–14]. Among them are, Flabeloic acid (**DAC**) and his dimer (**DACD**), as well as, Diepoxy-neoclerodane (**DiENC**), which were extracted from *Baccharis flabellata* [8–10]. Bartemidiolide oxide (**BARTO**) was obtained from *Baccharis artemisioides* [11]; and Hautriwaic acid (**HAW**) was obtained from *Baccharis crispa,* [12,13]. The lineal terpenoid Thymifodioic acid (**THYM**) was extracted from *Baccharis thymifolia* [14].

Significant antifeedant activities have been reported for some of these compounds [15–18] and more recently we reported antinociceptive effects for extracts obtained from *Baccharis flabellata* [19]. Our results suggest that this activity is mainly due to the presence of **DAC** and its dimer (**DACD**). We demonstrated that both compounds act on opioid receptors, being the antinociceptive effect of **DACD** stronger than **DAC**. We also conducted a molecular modeling study analyzing the molecular interactions of **DAC** and **DACD** complexes with the KORs.

Our results suggest interactions for both compounds with Gln115, Val118, Tyr119, Asn122, and Tyr313, which are stabilizing their complexes. In addition, our results indicate that these *neo*clerodanes would have a molecular mechanism of action similar to that of **SalA**; such information can be very useful for the design of new inhibitors of KORs. Based on our previous results and taking advantage of such data, in this work we have studied with more detail the antinociceptive activity of compounds **DAC** and **DACD**, but in this study, we have also included compounds structurally related to **DAC** (**BARTO**, **DiENC**, **HAW,** and **THYM**), to look for new molecules possessing this biological effect.

To better understand our experimental data, we have also performed a molecular modeling study by using docking calculations and molecular dynamics simulations for all the compounds reported here. In addition, considering that most of the anti-inflammatory clerodane diterpenoids have poor water solubility [20] and this property can be reduced for molecular aggregation, it is interesting to evaluate possible vehiculization of the compounds to improve pharmacodynamics aspects. We studied the incorporation of the most active compounds in nanovesicles formed by non-ionic surfactants (niosomes), looking for improving the bioavailability of these compounds.

2. Materials and methods

2.1. General experimental procedures

NMR spectra were measured at 400 MHz (^{1}H) and 100 MHz (^{13}C); chemical shifts are reported relative to internal Me_4Si ($\delta = 0$). NMR assignments were determined using 2D experiments (COSY, DEPT, HETCOR, HMBC, HSQC). Optical rotations were determined in $CHCl_3$. Column chromatography (CC) was performed on silica gel 60 Å (400–500 mesh), using increasing polarity *n*-hexane-EtOAc mixtures as solvent. Gel chromatography was carried out employing Sephadex LH-20 with MeOH as solvent. TLC was carried out on silica gel 60 F254 (0.2 mm thick plates) using a mixture of *n*-hexane-EtOAc (1:1) as solvent. Compounds were visualized using UV light and H_2SO_4-AcOH-H_2O (4:20:1) as chromogenic reagents. *Neo*-clerodanes were purified by Centrifugal thin layer chromatography (CTLC) on a Chromatotron

(Model 7924 T Harrison Research, Palo Alto, CA, USA). HPLC chromatography was carried out using a binary pump Waters® 1525 HPLC system (Milford, Massachusetts., USA) attached to a Waters® 2998 UV photodiode array detector. The column employed in all determinations was a C18 Chrompack® (packing material: Chromspher® C18 150 × 4.6 mm diameter, Santa Clara, California, USA). All solvents were purified by standard techniques.

2.2. Plant material and isolation of diterpenes

Aerial parts of *Baccharis artemisioides* (1 Kg) were collected in El Durazno Alto, San Luis, Argentina (33°07′35.2″S 66°08′37.9″W) at 1049 m AMSL (Del Vitto LA & EM Petenatti # 5301 UNSL). *Baccharis flabellata* aerial parts (2.3 Kg) were collected in Potrero de los Funes town, San Luis hills, Argentina (33° 11′ 90.88″ S, 66° 15′ 42.63″ W) at 1270 m AMSL. (Del Vitto LA & EM Petenatti 10520 UNSL). *Baccharis crispa* aerial parts (1.8 Kg) were collected in Río Grande, El Trapiche, San Luis, Argentina. (33°04′26″S, 66°09′56″O) at 1107 AMSL (UNSL 376). Aerial parts (2.8 kg) of *Baccharis thymifolia* were collected in Villavicencio, Mendoza, Argentina (32°31′37″S 69°01′06″O) at 2700 m AMSL (Del Vitto LA & EM Petenatti 9367 UNSL). All specimens were authenticated by Prof. Dr. Elisa Petenatti and each batch was deposited at the Herbarium of the Universidad Nacional de San Luis (L.A. Del Vitto & E.M. Petenatti). Leaves and stems were extracted with methanol in portions of 200 ml each, immediately after being cut from the plant at room temperature. The vacuum concentrate methanol extracts were subjected to a novel flash chromatography procedure using a combined stationary phase constituting successive layers of alumina (upper layer), activated charcoal (middle layer), and silica gel 60 (lower layer) (150 g each), to retain chlorophylls, flavonoids, and waxes, in a single procedure. Elution was performed with EA. The organic eluate, enriched in terpene compounds, was dried under vacuum yielding 185.30 mg of *Baccharis artemisioides*, 220.40 mg of *Baccharis flabellata,* 250.65 mg *of Baccharis crispa,* 210.13 mg, and 310.85 mg for *Baccharis thymifolia.* Solid materials obtained were resuspended in 10 ml of MeOH each and further separated by preparative CTLC. The CTLC plates were coated with a 2 mm thick layer of silica gel GF254 (Merck). The mobile phases used were increasing polarity mixtures of n-hexane (100%) to EA (100%) that were pumped at a flow rate of 1 ml min − 1. UV detection was carried out at 254 nm and 2 ml fractions were collected. *Neo*-clerodanes obtained were **BARTO** (50.10 mg) from *Baccharis artemisioides*, **DACD** (30.20 mg), **DAC** (39.20 mg), and **DiENC** (41.50 mg) from *Baccharis flabellata,* **HAW** (22.61 mg) from *Baccharis crispa* and **THYM** (17.34 mg) from *Baccharis thymifolia.*

2.3. Spectroscopic and spectrophotometric determinations

For all the compounds studied in this work, spectrometric and spectrophotometric data were in total agreement with those published lately by Tonn et al. for **BARTO** [11], Funes et al. for **DACD,** and **DAC** [9], Gianello and Giordano, for **DiENC** [10], Simirgiotis et al. for **HAW** [12], and Saad et al. for **THYM** [14].

More information is provided in supplementary data SI, Table S1 to S6, and Fig. S1 to S34. To assure solubility in $CDCl_3$, neoclerodanes whit acid substituents were derivatized with Ac2O/Py/DMAP, getting a pale-yellow oil.

2.4. HPLC–DAD characterization

2.4.1. For neoclerodanes determinations the photodiode array detector was working at the range of 200 nm to 750 nm

Standard solutions for every compound were made in methanol (10 mg ml^{-1}) and filtered through a Durapore® syringe membrane (Merck Millipore, Darmstadt, Germany) of 13 mm diameter and 0.22 μm pore size before the injection of 10 μl into the HPLC-DAD system. The C18 column was used at room temperature. The mobile phase consisting of MeOH 0.1% p/v aqueous acetic acid solution, in a proportion of 7:3 *v*/v, was used for isocratic elution at a flow rate of 1 ml min^{-1}. The total run time was 30 min and the detector was set at 296 nm (Fig. 2). For complete data, see HPLC conditions, chromatograms, and UV spectrums in SI, Fig.: S6, S12, S18, S24, S28, and S34.

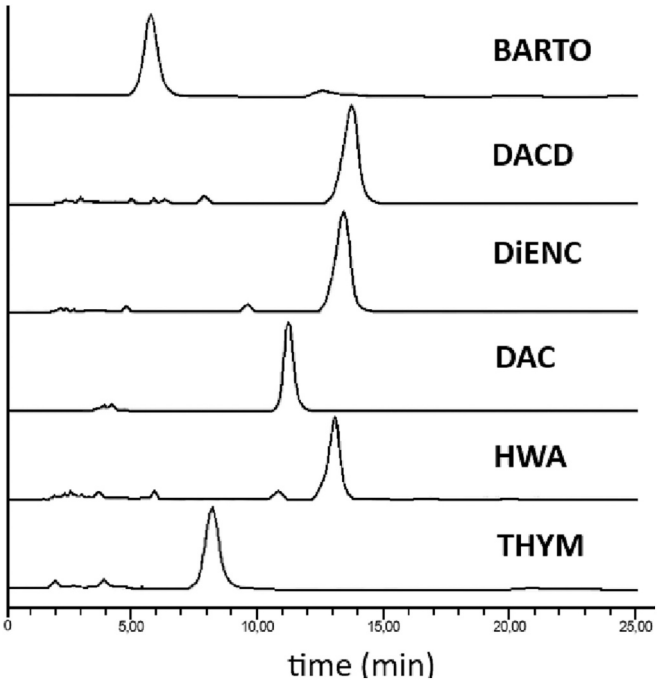

Fig. 2. HPLC-DAD profiles of purified neoclerodanes obtain from different species of *Baccharis* genus. The purity of each compound was ≥98%.

2.5. Bioassays

2.5.1. Animals

The experiments were performed on Rockland mice of either sex (25–30 g) with free access to standard food and water, in a 12 h day–night cycle (lights on from 07:00 to 19:00 h), at a constant temperature of (22 ± 3)°C (with periodic cycles of air changes) and relative humidity of about 50–60%. Acclimatization of animals was done for two days before the beginning of the experiment. The animals were randomly assigned to the different groups. All the animals were obtained from the Bioterium of the Facultad de Química, Bioquímica y Farmacia of Universidad Nacional de San Luis (Argentina) and the experiments complied with the ANMAT No. 64/96 [21]. Animal care guidelines were also authorized by Institutional Committee for the Care and Use of Laboratory Animals (Acronym: CICUA) of our institution (protocol No. F-206/15 in Resolution 324–16).

2.5.2. Antinociceptive activity

The hot-plate test was used to measure response latencies according to the method described by Eddy and Leimbach, with minor modifications [22]. Each mouse was placed on a hot plate kept at (56 ± 1) °C, after 30 min of animal injections. The latency in seconds was recorded using a stopwatch as the time between adjusting the animal on the hot plate and the appearance of symptoms of discomfort as licking of the hind paws, shaking, or jumping off from the surface. The reaction time was recorded before (0) and 0.5, 1, and 1.5 h after the treatments. The cutoff time of 60 s was selected according to Woolfe and MacDonald [23]. Mice with baseline latencies higher than 10 s were eliminated from the study. A significant increase in latency was considered indicative of analgesic activity. One group of animals was treated with **BARTO**, **DACD**, **DiENC**, **DAC**, **HAW,** and **THYM** at two doses (50 and 100 mg/kg,

i.p.), another group was given morphine (10 mg/kg, *s.c.*); while control animals received the same volume of saline solution (10 ml/kg *i.p.*). To assess the possible participation of opioid receptors, mice were pretreated with naloxone (100 mg/kg *i.p.*), a non-selective antagonist of opioid receptors.

2.5.3. Statistical analysis

Statistical analysis was performed using GraphPad Prism version 5.00 for Windows and GraphPad InStat version 3.00 for Windows (GraphPad Software, San Diego, CA, USA, www.graphpad.com). Data were indicated as the mean ± standard error of the mean (SEM). The statistical significance of differences between groups was assessed utilizing analysis of variance (ANOVA) and posterior comparison by Tukey. A probability of $p < 0.05$ was considered significant (section 4 of supplementary data).

2.5.4. KOR in vitro

Every cell line and experiment were utilized as previously delineated [24]. In summary, CHO-K1 cells that had a permanent expression of the human κ-opioid receptor were procured from Discoverx Corp. (Fremont, CA, USA; OPRK1 catalog no. 95-0088C2). Cells were implemented in the DiscoverX HitHunter cAMP analysis for small-molecule experimentation, following the instructions of the manufacturer, as thoroughly delineated [24].

2.6. Molecular modeling

2.6.1. Automated docking setup

The receptor structure corresponds to the following PDB code: 4DJH [25]. Missing residues Thr302, Ser303, His304, Ser305, and Thr306 have been included in the structure with Modeller 9.19 [26]. AutoDock Vina 1.1.2 [27] was used to dock each compound to the KOR and all graphic manipulations and visualizations were performed using AutoDock Tools 1.5.6 [28]. The receptor was defined as rigid and all torsions of the ligands were allowed to rotate during docking. The grid dimensions were 40, 40, and 40 for the X, Y, and Z axes, respectively, in the active site region with a resolution of 0.375 Å. Nonpolar hydrogen atoms were merged and Gasteiger charges were assigned for all the compounds. The value for the exhaustiveness of the search was 400, whereas the number of poses collected was 20.

2.6.2. MD simulations

MD simulations were performed using the AMBER16 software package [29]. For each complex, the three lowest energy conformations from docking calculations were considered to carry out the MD simulations using periodic boundary conditions and cubic simulation cells with explicit water, employing the TIP3P model [30]. Around 44,100 water molecules were added to the box, and chlorine ions were included to neutralize the system. The MD simulations were performed using the all-atom force field ff99SB [31] to describe the receptor, whereas the general Amber force field [32] was used to handle ligands and the force field parameters of the ligands were produced by the antechamber program in Amber. The particle mesh Ewald method (PME) [33] was applied using a grid spacing of 1.2 Å, a spline interpolation order of 4, and a real space direct sum cutoff of 10 Å. The SHAKE algorithm [34] was applied allowing for an integration time step of 2 fs. MD simulations were carried out at 310 K, and all alpha carbons from the protein backbone were kept almost fixed with a harmonic force constant of 500 kcal/mol $Å^{-2}$. Three MD simulations of 5 ns were conducted for each system under different starting velocity distribution functions; thus, in total 15 ns were simulated for each complex. The NPT ensemble was employed using Berendsen coupling to a baro/thermostat (target pressure 1 atm, relaxation time 0.1 ps). Post MD analysis was carried out with the program CPPTRAJ [35]. Spatial views shown in Figs. 4 and 6 were constructed using the UCSF Chimera program as a graphic interface [36].

2.6.3. MM-GBSA free energy decomposition

Interaction energy histograms were used to determine which KOR residues were involved in the interactions with the ligands. For this purpose, we have employed MM-GBSA free energy decomposition using the mm_pbsa program [37] in AMBER16. This calculation allowed decomposing the interaction energies to each residue considering molecular mechanics and solvation energies [38]. Four energy terms were included for each ligand-residue pair: van der Waals contribution (ΔE_{vdW}), electrostatic contribution (ΔE_{ele}), polar desolvation term (ΔG_{GB}), and nonpolar desolvation term (ΔG_{SA}), which can be summarized as the following equation:

$$\Delta G_{ligand-residue} = \Delta E_{vdw} + \Delta E_{ele} + \Delta G_{GB} + \Delta G_{SA} \quad (1)$$

For MM-GBSA methodology, snapshots were taken at 10 ps time intervals from the corresponding last 2000 ps MD trajectories, and the explicit water molecules were removed from the snapshots.

2.7. Incorporation of neoclerodanes in niosomes

Because **BARTO** and **DACD** are the most active compounds, were vehiculated in soft materials as a particular type of vesicles, called niosomes, obtained from non-ionic surfactants derived from renewable sources, and approved for use in food and pharmaceutical applications. Niosomes were prepared in an equimolar mixture of tween 80 (Tw80) and span 80 (Sp80) in water (total working concentration = 10 mM) using the thin film hydration method followed by extrusion through a 100 nm membrane as was previously described [39]. Briefly, stock solutions of Tw80, Sp80, and these most active neoclerodanes in EtOH were prepared. Appropriate aliquots of non-ionic surfactants and active neoclerodanes solutions (to obtain a final concentration of 10 mM and 0.22 mM respectively) were added in a round bottom flask. Then, EtOH was completely removed under reduced pressure in a Büchi R-200 equipment, until a thin film was formed on the flask walls. After that, MilliQ water (10 ml) was added and the suspension was shaken at 116 spm at 60 °C in a shaker water bath for 30 min (OLS200 Grant). The dispersion was left to equilibrate at room temperature overnight. The final suspension was extruded 21 times through a 100 nm pore size polycarbonate membrane using a manual mini extruder from Avanti Polar Lipids, Inc. Subsequently, BARTO-niosomes and DACD-niosomes were separated from free active neoclerodanes using size exclusion gel chromatography (14.5 × 50 mm Disposable Desalting Column with Sephadex G-25 resin, GE Healthcare Life Sciences). Extruded vehiculated active neoclerodanes were used for further analysis. To quantify the amount of NCD inside the niosomes, a sample (0.1 ml) was diluted in MeOH (1 ml), and the absorbance at 305 nm was recorded on Waters HPLC-DAD chromatographer. The NCD concentration was determined via interpolation from a separate calibration curve.

Encapsulation efficiency (*EE*) was determined as the percentual ratio between the quantity of encapsulated neoclerodane (remaining after purification using exclusion gel chromatography) and the total compound added during niosome preparation as the following equation (Eq. (2)):

$$EE = \frac{[neo-clerodanes]_{encapsulated}}{[neo-clerodanes]_{total\ added}} \times 100 \quad (2)$$

Release experiments were performed under simulated gastrointestinal conditions at 37 °C using Franz diffusion cells. To achieve gastric conditions, a buffer solution at pH 1.2 was prepared with HCl/KCl, 0.085 M/0.050 M, and to imitate intestinal conditions, a buffer at pH 6.8 was prepared with $NaOH/KH_2PO_4$, 0.022 M/0.050 M, as was previously described [40]. The donor compartment of the cell was filled with neoclerodanes loaded niosomes whereas the receptor compartment was filled with the corresponding buffer solution. Both compartments were separated with a dialysis benzoylated membrane (Sigma Aldrich, cutoff 2 kDa MW). At specific time intervals (for 2 h at pH 1.2 and 6 h at pH

Table 1
The effect of cyclic and linear diterpenes and morphine by intraperitoneal (*i.p.*) or subcutaneous (s.c.) route of administration in the hot plate test. The latency for the nociceptive behavior was recorded before 0, 15, 30, 60, and 90 min after the treatments. All values were expressed as mean ± standard error of the mean (SEM). Asterisks denote significant differences from the control: ***$p < 0.001$ vs. control (ANOVA and posterior comparison by Tukey test).

Treatment	Dose (mg/kg)	0 min.	15 min.	30 min.	60 min.	90 min.
BARTO	25 *i.p.*	7.45 ± 0.62	8.27 ± 0.85	16.25 ± 1.21***	19.02 ± 1.36***	28.74 ± 2.12***
	50 *i.p.*	7.98 ± 0.54	18.16 ± 1.23***	27.08 ± 1.88***	35.22 ± 2.02***	44.27 ± 2.02***
	100 *i.p.*	7.84 ± 1.21	25.01 ± 1.14***	39.07 ± 0.99***	50.03 ± 1.39***	52.20 ± 1.02***
DACD	25 *i.p.*	6.83 ± 0.36	6.47 ± 0.97	9.01 ± 1.24	12.17 ± 2.20	19.14 ± 1.27 ***
	50 *i.p.*	7.61 ± 0.36	11.43 ± 1.13	22.14 ± 1.42***	28.41 ± 2.34***	35.21 ± 1.02 ***
	100 *i.p.*	7.64 ± 1.09	22.86 ± 2.26***	36.38 ± 2.94***	44.81 ± 3.68***	49.43 ± 2.08***
DiENC	25 *i.p.*	6.02 ± 0.12	7.71 ± 1.49	7.98 ± 3.16***	13.65 ± 1.75	15.82 ± 1.00***
	50 *i.p.*	5.98 ± 0.08	9.65 ± 1.97	16.77 ± 3.16***	27.28 ± 1.75***	36.27 ± 1.20***
	100 *i.p.*	7.98 ± 1.08	18.65 ± 2.97***	26.77 ± 5.16***	37.28 ± 2.75***	46.27 ± 2.20***
DAC	25 *i.p.*	7.45 ± 0.04	7.65 ± 0.08	8.01 ± 0.52	9.27 ± 0.34	12.17 ± 1.65
	50 *i.p.*	7.97 ± 0.08	9.34 ± 0.13	10.03 ± 0.33	15.30 ± 0.24	20.12 ± 2.12***
	100 *i.p.*	7.77 ± 1.27	16.68 ± 1.36***	21.09 ± 0.99***	24.60 ± 1.39***	36.14 ± 3.23***
HWA	25 *i.p.*	7.11 ± 0.76	7.98 ± 0.63	8.33 ± 0.84	9.74 ± 1.28	12.72 ± 1.56
	50 *i.p.*	7.15 ± 0.66	8.35 ± 0.63	10.53 ± 0.68	15.64 ± 1.12	19.64 ± 1.12***
	100 *i.p.*	7.52 ± 1.39	17.99 ± 2.10***	20.21 ± 1.73***	22.33 ± 2.59***	37.33 ± 1.86***
THYM	25 *i.p.*	4.21 ± 0.22	3.76 ± 0.46	9.01 ± 0.75	5.48 ± 0.41	4.32 ± 0.11
	50 *i.p.*	3.99 ± 0.25	5.88 ± 0.63	10.36 ± 0.68	7.26 ± 0.56	6.52 ± 0.24
	100 *i.p.*	8.17 ± 1.32	18.78 ± 0.66***	22.27 ± 1.06***	19,37 ± 0.50***	14.45 ± 0.53
Morphine	10 *s.c.*	8.09 ± 0.92	35.00 ± 1.63***	41.85 ± 1.21***	52.12 ± 2.20***	54.71 ± 1.25***
Control	Saline phys. Sol. *i.p.*	7.96 ± 0.37	8.20 ± 0.36	8.78 ± 0.25	8.43 ± 0.32	7.83 ± 0.41

6.8), an aliquot was carefully removed for subsequent HPLC-DAD analysis to evaluate the clerodane concentration. The removed volume was replaced with a fresh buffer solution. The compound concentration was determined from a calibration curve and the cumulative release was obtained by calculating the total amount detected in the aliquots.

3. Results and discussion

3.1. Antinociceptive activities

Based on our previous information about the structural requirements for these compounds to produce antinociceptive activity, we have selected for this study the compounds shown in Fig. 1B.

Compounds **DACD** and **DAC** were taken as starting structures due to their structural resemblance with **SalA** and their antinociceptive activities were previously reported [19]. In the same way, **BARTO**, **DiENC,** and **HAW** were chosen and their antinociceptive activities were compared with **DACD**. In addition, in this study, we wanted to evaluate one compound possessing a higher molecular flexibility, and therefore, **THYM** (a linear diterpene) was also included.

Antinociceptive activities of cyclic and linear diterpenes are shown in Table 1. In this series, it is clear that **BARTO** is markedly more active than **DACD** at 50 and 100 mg/kg applied *i.p.* **DAC** and **HWA** have shown weaker activity than **BARTO**, but their activities are still significant. **DiENC** presents higher activity compared whit **DAC** and **HWA,** especially at 100 mg/kg applied *i.p.* Linear diterpene, a very flexible compound, presents a similar activity at both concentrations, closer to that of **DAC** 50 mg/kg applied *i.p.*

This type of compound could contribute to a new perspective on the antinociceptive activity of diterpenes and could be applied to cases of moderate sedation [41]. In this work, we continued with the study of the antinociceptive activity mechanism applied for other diterpenes (neoclerodanes) similar to **SalA** as **BARTO** and linear diterpenes as **THYM**.

Antinociceptive mechanism of **BARTO, DiENC, HWA,** and **THYM** was reversed by prior administration of naloxone (1 mg/kg, *i.p.*), a non-selective antagonist of opioid receptors (Fig. 3), suggesting that the opioidergic mechanism is involved in the antinociceptive action of **DAC** and **DACD** [19].

At this point of our study, we considered it very important to determine the possible mechanism of action at the molecular level of these compounds. Thus, considering the structural resemblance between **BARTO** and **DiENC** with **SalA**, as well as, the activities previously reported for several neoclerodanes on the KOR, it is reasonable to think that these neoclerodanes could be acting against the same molecular target and through the same mechanism of action. To better understand these results, we simulated the interaction of cyclic and linear diterpenes at the active site of KOR. Thus, we carried out a molecular modeling study for these compounds and such results are discussed in the next section.

3.2. KOR in vitro activity

We perform an in vitro functional assay to assess the inhibition of forskolin-induced cAMP accumulation in CHO cells to stably express the hKOR for neoclerodane diterpene compounds of different *Baccharis* genus. SalA is a full KOR agonist with a potency of 0.042 ± 0.005 nM [42], therefore, **THYM**, **HAW,** and **DAC** do not demonstrate KOR activity at 50 μM. (Table 2). The most promising compounds should be those that presented greater antinociceptive activity shown in Table 1. However, according to the Table 2, **BARTO**, **DiENC,** and **DACD** did not approach the potency of **SalA**, with their potency values are 19.0 ± 0.6 μM, 27.0 ± 0.6 μM, and 33.0 ± 0.6 μM respectively. Although activities obtained for compounds reported here are significantly weaker than that of **SalA**, our results confirm that the most potent neoclerdanos as antinociceptives, express in good proportion the hKOR, effect: being **BARTO** the most active as KOR inhibitor.

3.3. Molecular modeling

To perform this study, we used combined techniques of docking and MD simulations, which allowed us to determine the molecular interactions of these compounds at the molecular target (the KORs). In this

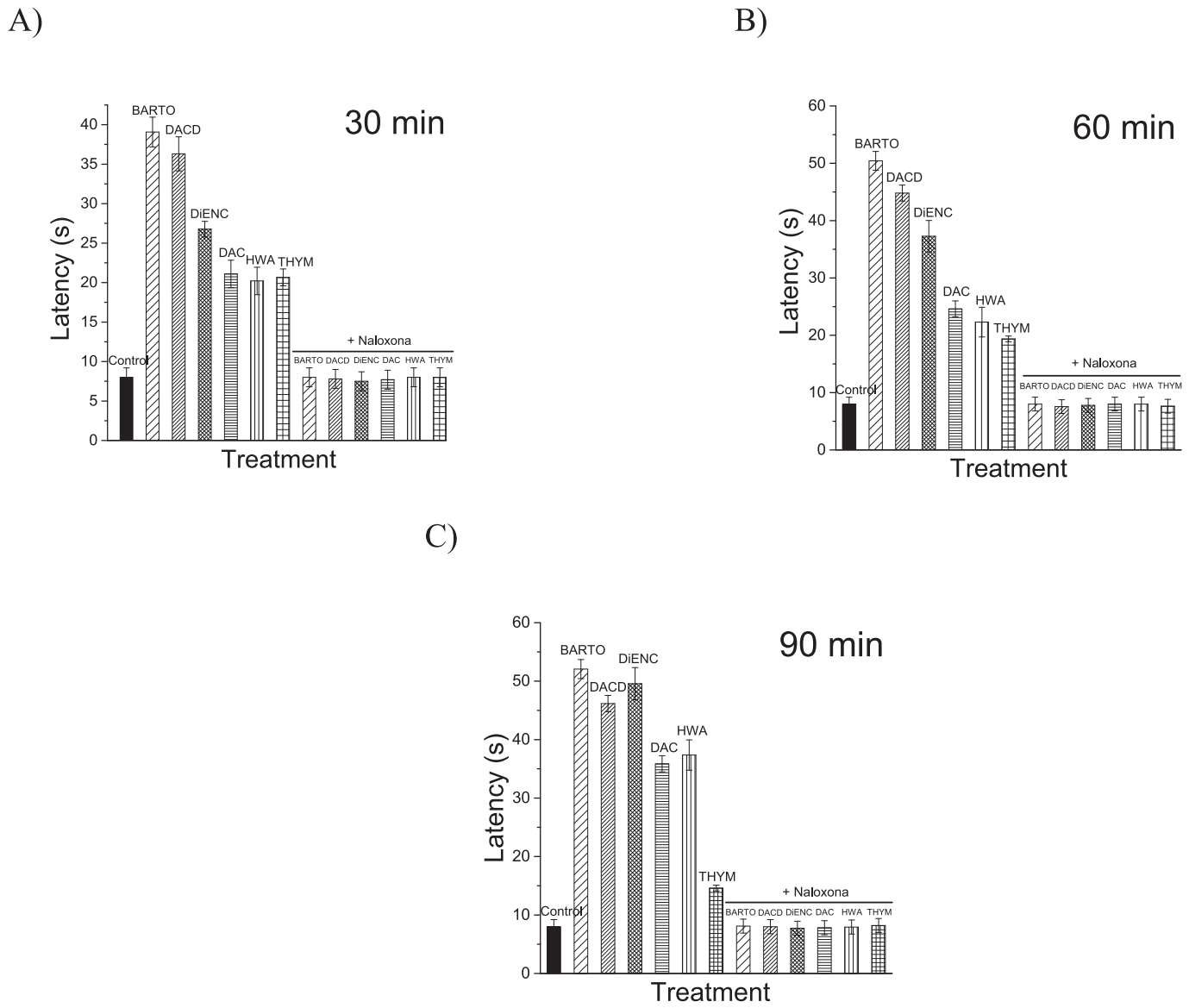

Fig. 3. Effect of cyclic and linear neoclerodanes on hot plate test at 30, 60, and 90 min ($n = 7$) and pretreatment with naloxone (1 mg/kg, i.p.). Values are expressed as mean ± SEM, where $^{***}p < 0.001$ vs. **BARTO, DACD, DiENC, DAC, HWA,** and **THYM** alone and $^{###}p < 0.001$ vs. control, according to ANOVA, followed by Tukey's test.

Table 2
In Vitro KOR Activity results.

Compound	potency EC50 ± SEM[a,b] (μM)
BARTO	19.0 ± 0.6
DACD	27.0 ± 1.5
DiENC	33.0 ± 2.1
DAC	>50[c]
HWA	>50[c]
THYM	>50[c]

SalA EC50 = 0.042 ± 0.005 nM and Emax =100%.
[a] means ± standard error of the mean; $n \geq 2$ individual experiments run in triplicate [42].
[b] KOR Emax = 100% unless otherwise noted.
[c] KOR Emax = 0% up to 50 μM.

study, we have also included **SalA** for comparison reasons. As was previously denoted, **SalA** is a natural neoclerodane with a potent opioid analgesic effect [6] and is structurally related to the compounds reported here.

Our simulations combining docking study and MD calculations, indicated that **BARTO**, **DiENC**, **HAW,** and **THYM** bind in the same region of the active site of KOR as that previously reported for **SalA** [7], **DAC,** and **DACD** [19] (Fig. 4). Although in general docking calculations have some limitations [23,24], in this case, they provide very interesting information.

Our docking results clearly showed the high molecular flexibility of **THYM,** even within the active site of the KOR. **THYM** shows, in its structure (Fig. 1B), a large number of spatial arrangements, that might adopt in the binding pocket. Considering the high number of different poses obtained for **THYM**, it is very difficult to take clear criteria to select the better candidates to bind into the molecular target. However, this behavior is different from those obtained for the rest of the compounds, which displayed quite a low molecular flexibility. The docking results obtained for **BARTO** are shown in Fig. 5B. In this case, there is a highly preferred family considering population and energy scores. Similar results to **BARTO** were obtained for **DACD** and **DiENC**. This different behavior could explain at least in part the lack of activity

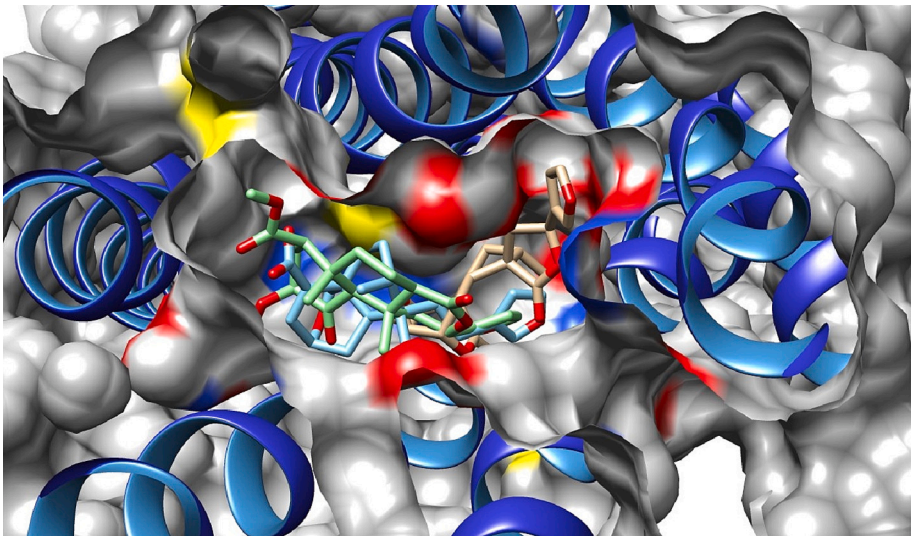

Fig. 4. Spatial view for the superimposition of the **SalA** (green), **BARTO** (tan), and **DiENC** (light blue) in the binding site of KOR. (For interpretation of the references to colour in this figure legend, the reader is referred to the web version of this article.)

shown by **THYM** compared to the rest of the compounds in the series. Based on these results, we focused our interest on **BARTO**, **DACD,** and **DiENC**; thus, in the next stage, we performed an analysis per residue for such compounds. These results were compared with those previously reported for **SalA**. (Fig. 5A) experiments complied with the ANMAT) shows the analysis per residue obtained for the different complexes.

Analyzing in detail our results, MD simulations indicated that these molecules are arranged spatially in a slightly different way to that of **SalA** at the binding site, which could explain the different activities observed in this series. From Fig. 5 it can be seen that the three compounds interact mostly with the same residues: Asp138, Met142, Ile 290 Tyr312, and Ile316. However, there are some differences, for example, **BARTO** shows interactions with Gln115 (as does **SalA**); while **DACD** and **DiENC** do not present this interaction. Another notable difference is that **DACD** and **DiENC** have a significant interaction with Lys227, while **BARTO** does not show this interaction. It should be noted that **SalA** establishes both types of interactions (with Gln115 and Lys227).

Based on our results, it could be speculated that the interaction with Gln115 is more important than that with Lys227 since **BARTO** has remarkably stronger inhibitory effects than that **DACD** and **DiENC**, however, we must be cautious with this comment. It is more prudent to think that both interactions could be important to have a strong biological effect. Anyway, comparing the spatial arrangements obtained for these compounds, our results indicate that **BARTO** adopts a spatial ordering quite similar to that of **SalA** (Fig. 6), which could explain its stronger activity concerning the other compounds studied here. In addition, interesting information can be obtained from MD simulations by analyzing the values of binding energies obtained for the different complexes (Table 3).

In general, there is a good correlation between the binding energy values obtained for the different complexes and the antinociceptive effect shown by these compounds. **SalA**, which is undoubtedly the most active compound, has the highest value (−37.56 kcal/mol), followed by **BARTO** (−33.24 kcal/mol) which is the most active compound in this series. At the other extreme, the less active compounds **DAC** and **HWA** show the lowest values; while **DACD** and **DiENC** have intermediate (and fairly close) values. It is interesting to note that these values obtained through simulations are in line with the experimental data obtained.

3.4. Vehiculization of neoclerodanes in niosomes

Pharmacokinetics properties of compounds are as important as their pharmacodynamics characteristics. High oral bioavailability is an important point to consider for the development of bioactive molecules as therapeutic agents. Compared to many synthetic compounds and natural products, the logP value of clerodane diterpenoids is higher, indicating lower oral bioavailability [20]. Most of the anti-inflammatory clerodanes have poor water solubility. These characteristics compromise the oral bioavailability of the compounds. Poor oral bioavailability can result in variable exposure to active drugs, especially when the factors that limit it are compromised in a specific individual [43].

In this context, to improve the pharmacokinetic characteristics of **DACD** and **BARTO,** we have encapsulated them in soft nanomaterials as niosomes. Although the vehiculization of clerodanes using niosomes was not found in the literature, a single example was found using *trans*-dehydrocrotonin (t-DCTN) into liposomes [44]. Other drugs with anesthetic activity such as morphine and opiorphin were encapsulated in a wide range of liposomal formulations [45–47] while niosomes were employed for classical anesthetic drugs such as lidocaine [48].

Niosomes are vesicles composed of non-ionic surfactants that consist of concentric hydrophobic bilayers enclosing an inner aqueous compartment. Niosomes offer advantages over other vesicular systems, such as biocompatibility, chemical stability, and low cost, among others [49]. In these systems, lipophilic molecules remain entrapped within the lipidic bilayer, whereas more water soluble ones are preferably located in the internal aqueous core compartment. In this work, niosomes were formulated with Tw80:Sp80 (1:1) as were previously characterized [39] which are surfactants approved for their use in foods and pharmaceutical applications.

The encapsulation efficiencies (EE) values for the incorporation of **DACD** and **BARTO**, determined after the purification of the niosomes by size exclusion gel chromatography were 72% and 50% respectively. There are very few examples of the use of vesicular systems to encapsulate clerodanes. For instance, Lapenda et al. encapsulated t-DCTN and its inclusion complexes with hydropropyl-β-cyclodextrin (HP-β-CD) in liposomes, to improve t-DCTN antitumor activity. They obtained better values of EE than in this work, (about 90%) showing better interaction of the compound with liposomes [44]. Other authors reported encapsulation efficiencies for opiorphin (an endogenous regulator peptide with a strong pain killing effect) of around 90 and 70% using conventional and PEGylated liposomes, respectively [47].

The release of both clerodanes from niosomes was measured at 37 °C at pH 1.2 (to emulate gastric conditions) and pH 6.8 (to mimic intestinal conditions), considering oral administration. The release of **DACD** from niosomes was very scarce in both media, reaching 13% at pH 1.2 during 2 h and 1.8% at pH 6.8 in 6 h. The differences were probably related to

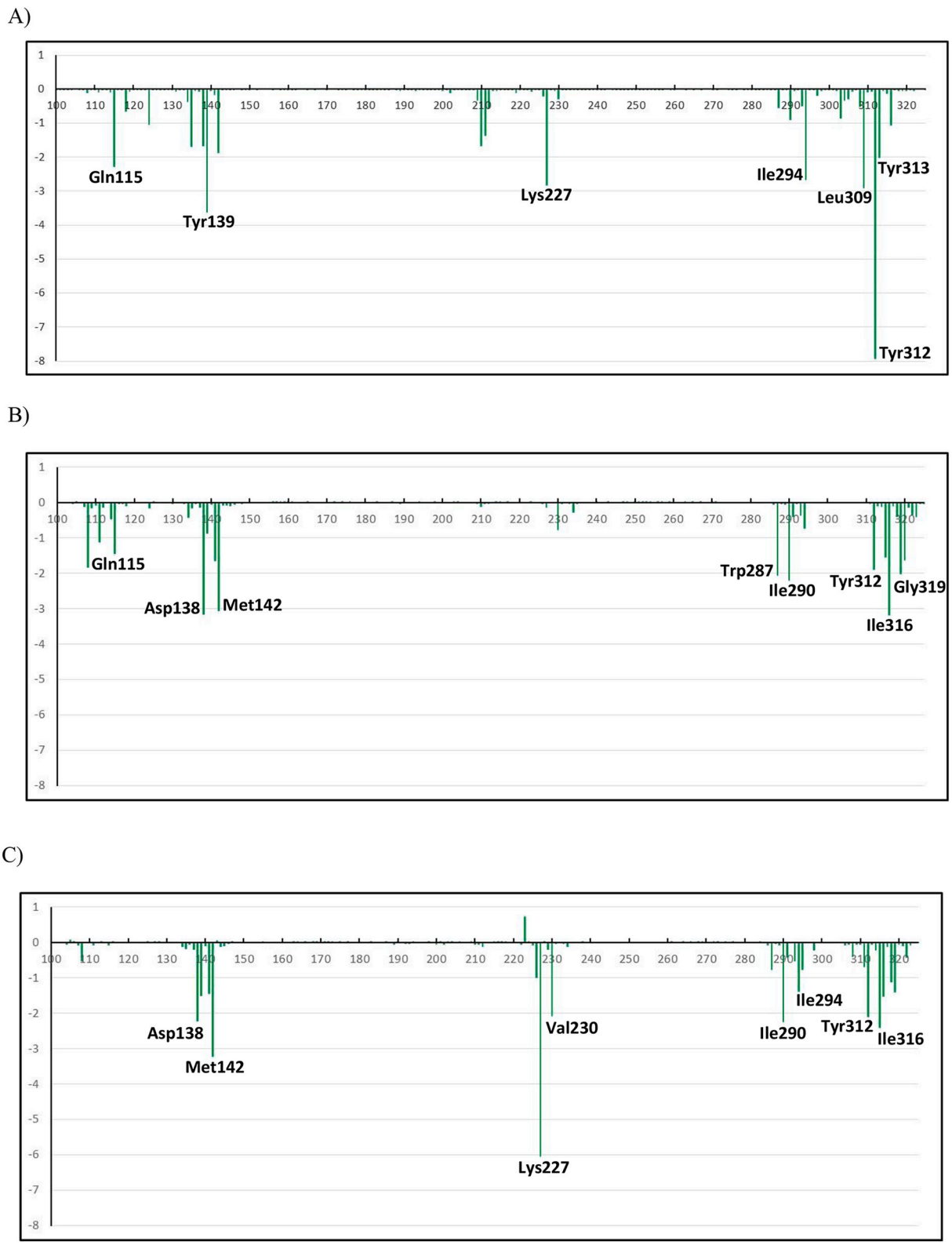

Fig. 5. Histograms of interaction energies partitioned concerning the KOR amino acids in complex with A) **SalA**, B) **BARTO,** and C) **DiENC**. The *x-axis* denotes the residue number of KOR, and the *y-axis* denotes the interaction energy between the compounds and a specific residue. Negative values and positive values are favorable or unfavorable to binding, respectively.

different acid-base species at both pH, due to the ionization of carboxylic acids moieties in the **DACD** molecule. Besides, the interaction of this clerodane with the niosomes bilayer seems to be strong, hindering the release in the studied time. On the contrary, **BARTO** release was higher at both pH conditions (43% at pH 1.2 after 2 h and 47% at pH 6.8 in 6 h). **BARTO** resulted in the most active compound of the molecules studied, and also showed higher release from niosomes. Previously, other authors encapsulated morphine (an opioid agonist) into liposomes, and a

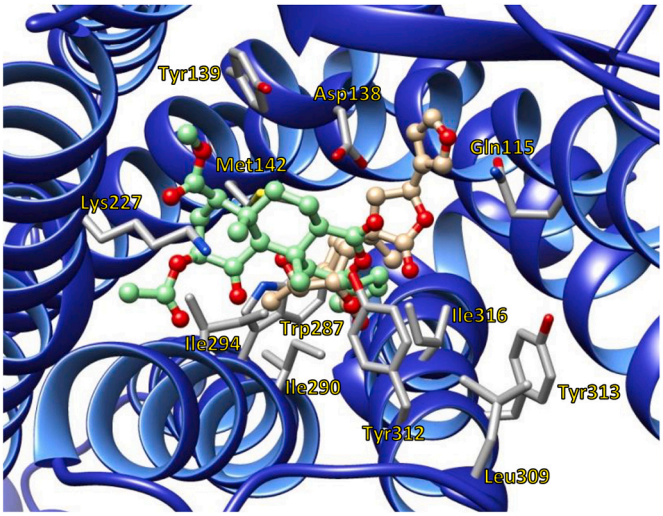

Fig. 6. Spatial view of the binding site of KOR with **SalA** (green) and **BARTO** (tan). The main residues of the active site are highlighted. (For interpretation of the references to colour in this figure legend, the reader is referred to the web version of this article.)

Table 3
Binding energies obtained from MD simulations for the different L-R complexes.

Compound	Binding energy (kcal/mol)
SalA	−37.56
BARTO	−33.24
DiENC	−29.77
HAW	−25.04
DAC	−21.08
DACD	−27.78

more prolonged release was observed. Almost 40% of the drug was released after 60 h from liposomes made of soybean lecithin [47] and 43% after 24 h from unilamellar liposomes covered by a PEG layer [44] at physiological pH. The presence of a portion of cationic morphine (pKa 8.1) at pH 7.4 could improve the interaction with the phosphate moieties present in the lipid membrane, retarding the drug release in comparison with the clerodanes employed in this work. Lidocaine, another anesthetic drug, was previously encapsulated into pH-sensitive niosomes based on Tween 20 derivatized by glycin and in this case, ~35% of the drug was released at pH 7.4 after 6 h [48].

The evaluation of in vitro release kinetics of active substances from delivery systems plays an important role in predicting and management of their efficacy and safety [49]. In this sense, release plots were fitted according to different empirical equations, zero and first order kinetics, Higuchi, and Korsmeyer-Peppas models (to see Eqs. 3–6). There M_t and M_∞ correspond to the cumulative and the maximal amounts of active compound released at time t, respectively. In the zero order kinetics, the fraction of drug release is proportional to the time, with a rate constant (Eq. 3) while in the first order kinetics model (Eq. 4), is the natural logarithm of the fraction of drug released proportional to the time. In the Higuchi model (Eq. 5), the fraction of the drug released is proportional to the square root of time, and K is a constant related to the formulation. Regarding the Korsmeyer-Peppas model (Eq. 6), k is the rate constant and n is the exponent that characterizes the release mechanism (e.g., $n = 0.5$ corresponds to a Fickian diffusion mechanism, whereas $0.5 < n < 1$ is typical for non-Fickian diffusions).

$$\frac{M_t}{M_\infty} = k^* t \tag{3}$$

$$Ln\frac{M_t}{M_\infty} = k^* t \tag{4}$$

$$\frac{M_t}{M_\infty} = k^* \sqrt{t} \tag{5}$$

$$\frac{M_t}{M_\infty} = k^* t^n \tag{6}$$

The kinetic parameters calculated from the empirical models are shown in Table 4. The correlation coefficients (R^2) indicated that the best-fitted model for the release of **BARTO** from the niosomes was the Zero order model. This result indicated that **BARTO** release was independent of its initial concentration with a constant release rate. This type of kinetic profile is useful to minimize dosing variation [50]. However, the release rate constants obtained for **BARTO** were ca 4-fold faster at pH 1.2 than at 6.8. At a strongly acidic medium, the ester moieties presented in **BARTO** may hydrolyze and thus increase its hydrophilicity, favoring the release from the niosomes to the aqueous medium. Nevertheless, more studies are needed to ensure this hypothesis. In the case of **DACD**, the best-fitted kinetic model was the Higuchi one, indicating that **DACD** release was governed by the diffusion with absence of vesicle disintegration [49–51]. Similar behavior was found for the release of t-DCTN and its inclusion complex from liposomes at pH 7.4 which also showed a release profile according to the Higuchi model, with a burst effect in the first 2 h and then a prolonged release of the drug (90% in 24 h) [42]. In the present work, the slow diffusion of **DACD** from the niosomes may be related to its high molecular weight in comparison with **BARTO** and the higher contribution of lipophilic moieties in the chemical structure, which could favor the partition to the noisome bilayer than to the release media.

4. Conclusions

There is a clear demand for new agonists of the KORS and in such target the trend towards the use of natural products as medicines, instead of synthetic drugs is an important alternative for the development of new specific agonists of the KORs. We report here the antinociceptive activity displayed by *neo*-clerodane diterpenes obtained from the *Baccharis* genus; such activities are relatively strong, particularly that observed for **BARTO**.

Our molecular modeling study has allowed us to understand the possible mechanism of action of **BARTO**. Combined docking and MD simulations suggest that compounds reported here might share the molecular action mechanism reported for **SalA**. Such a result is not unexpected considering the structural resemblance between **SalA** and

Table 4
Release kinetics model parameters for **DACD**-niosomes and **BARTO**-niosomes under simulated gastrointestinal conditions at 37 °C.

Delivery system	pH release medium	Zero order		First order		Higuchi		Korsmeyer-Peppas		
		k	R^2	k	R^2	k	R^2	k	R^2	n
DACD-niosomes	1.2	8.88	0.8446	3.80	0.5497	17.31	**0.9032**	8.79	0.8373	0.8049
	6.8*	–	–	–	–	–	–	–	–	–
BARTO-niosomes	1.2	32.94	**0.9926**	2.05	0.9268	59.48	0.9709	22.46	0.8889	1
	6.8	8.39	**0.9852**	0.44	0.9515	28.42	0.9443	4.60	0.3351	1

* The release of DACD from niosomes at pH 6.8 was very low.

some of the compounds reported here. In particular, molecular simulations have allowed us to appreciate some subtle differences between molecular interactions of these ligands stabilizing their respective complexes; such information might be useful for designing new inhibitors of KORS.

The incorporation of clerodanes diterpenes in niosomes resulted in important differences in the release of the compounds. The fit of the data to different models indicated that the drug release kinetics depends on the media's pH but also the type of clerodane. Moreover, this release was controlled with the absence of burst release. **BARTO**, as the most bioactive clerodane, showed a Zero order kinetic model which ensures a constant drug release after a single dose administration.

Our results indicate that **BARTO** could be an interesting starting structure for the search and development of new analgesic agents which could end up with serious side-effects caused by morphine analgesic treatment, such as addictive tendency, among others.

Declaration of Competing Interest

The authors have no conflict of interest.

Acknowledgements

- Dr. Matias Funes thanks Herbarium UNSL, Dr. Luis Del Vitto, and Dra. Elisa Petenatti for vouchers of each species studied. Grants from Universidad Nacional de San Luis (UNSL-Argentina) (PROICO: 02-1220) partially supported this work.
- Dr. Ricardo Daniel Enriz thanks ANPCyT for grants (PICT 2018-03259) which supported this work. Grants from Universidad Nacional de San Luis (UNSL-Argentina) (PROICO: 02-1418) partially supported this work.
- Dr. David Díaz Díaz thanks the Spanish Government for the Senior Beatriz Galindo Award (BEAGAL18/00166) and the project PID2019-105391GB-C21/AEI/10.13039/501100011033, as well as NANOtec, INTech, Cabildo de Tenerife and ULL for laboratory facilities.

Appendix A. Supplementary data

Supplementary data to this article can be found online at https://doi.org/10.1016/j.fitote.2023.105622.

References

[1] R. Telugunta, K. Urde, Pain Management Drugs Market, Editorial Bureaus, 2022.
[2] M. Comelon, J. Raeder, T. Drægni, M. Lieng, H. Lenz, Tapentadol versus oxycodone analgesia and side effects after laparoscopic hysterectomy: a randomized controlled trial, Eur. J. Anaesthesiol. 38 (2021) 995–1002, https://doi.org/10.1097/EJA.0000000000001425.
[3] H. Pathan, J. Williams, Basic opioid pharmacology: an update, Br. J. Pain 6 (2012) 11–16, https://doi.org/10.1177/2049463712438493.
[4] M.L. Naour, M.M. Lunzer, M.D. Powers, A.E. Kalyuzhny, M.A. Benneyworth, M. J. Thomas, S.P. Portoghese, Putative kappa opioid heteromers as targets for developing analgesics free of adverse effects, J. Med. Chem. 57 (2014) 6383–6392, https://doi.org/10.1021/jm500159d.
[5] M. Guerrero, M. Urbano, E.K. Kim, A.M. Gamo, S. Riley, L. Abgaryan, N. Leaf, L. J. Van Orden, S.J. Brown, J.Y. Xie, F. Porreca, M.D. Cameron, H. Rosen, E. Roberts, Design and synthesis of a novel and selective kappa opioid receptor (KOR) antagonist (BTRX-335140), J. Med. Chem. 62 (2019) 1761–1780, https://doi.org/10.1021/acs.jmedchem.8b01679.
[6] J. Listos, A. Merska, S. Fidecka, Pharmacological activity of Salvinorin a, the major component of *Salvia divinorum*, Pharmacol. Rep. 63 (2011) 1305–1309, https://doi.org/10.1016/s1734-1140(11)70694-6.
[7] A.P. Riley, C.E. Groer, D. Young, A.W. Ewald, B.M. Kivell, T.E. Prisinzano, Synthesis and κ-opioid receptor activity of furan-substituted salvinorin a analogues, J. Med. Chem. 57 (2014) 10464–10475, https://doi.org/10.1021/jm501521d.
[8] J.R. Saad, J.G. Davicino, O.S. Giordano, A diterpene and flavonoids of *Baccharis flabellata*, Phytochem. 27 (1988) 1884–1887, https://doi.org/10.1016/0031-9422(88)80471-0.
[9] M. Funes, C.E. Tonn, M. Kurina-Sanz, In vivo photoinduced [4+2] dimerization of a *neo*-clerodane diterpene in *Baccharis flabellata*. ROS and RNS scavenging abilities, J. Photochem. Photobiol. B 186 (2018) 137–143, https://doi.org/10.1016/S0031-9422(02)00241-8.
[10] V.E. Juan Hikawczuk, P.C. Rossomando, O.S. Giordano, J.R., Saad, *neo*-Clerodane diterpenoids from *Baccharis flabellata*, Phytochem. 61 (2002) 389–394, https://doi.org/10.1016/S0031-9422(02)00241-8.
[11] C.E. Tonn, O.S. Giordano, R. Besalle, F. Frolow, D. Lavie, The structure of bartemidiolide a clerodane-type diterpene from *Baccharis artemisioides*, Phytochem. 27 (1988) 489–491, https://doi.org/10.1016/0031-9422(88)83127-3.
[12] C.E. Tonn, J.C. Gianello, O.S. Giordano, Bacrispine: a new diterpene isolated from *Baccharis crispa* Sprengel, An. Assoc. Quím. Argent. 67 (1979) 1–8.
[13] C.E. Tonn, O.S. Giordano, A new Furane Diterpenoid from *Baccharis crispa* Sprengel, An. Assoc. Quím. Argent. 68 (1980) 237–241.
[14] J.R. Saad, M.J. Pestchanker, O.S. Giordano, Furanediterpenes from *Baccharis thymifolia*, Phytochem. 26 (1987) 3033–3035.
[15] A. González-Colomaa, A. Guadaño, C.E. Tonn, M.E. Sosa, Antifeedant/insecticidal terpenes from Asteraceae and labiatae species native to Argentinean semi-arid lands, ZNC 60 (2005) 855–861, https://doi.org/10.1515/znc-2005-11-1207.
[16] P.I. Bozova, Y.P. Georgieva, Antifeedant activity of *neo*-clerodane Diterpenoids from *Scutellaria altissima* against Colorado potato beetle larvae, Nat. Prod. Commun. 12 (2017) 327–328, https://doi.org/10.1177/1934578X1701200303.
[17] R.D. Enriz, H.A. Baldoni, M.A. Zamora, E.A. Jáuregui, M.E. Sosa, C.E. Tonn, J. M. Luco, M. Gordaliza, Structure antifeedant activity relationship of clerodane diterpenoids. A comparative study with withanolides and azadirachtin, J. Agric. Food Chem. 48 (2000) 1384–1392, https://doi.org/10.1021/jf990006b.
[18] R.D. Enriz, H.A. Baldoni, E.A. Jauregui, M. Sosa, C. Tonn, O.S. Giordano, Structure activity relationship of Clerodane Diterpenoids acting as Antifeedant agents, J. Agric. Food Chem. 42 (12) (1994) 2958–2963, https://doi.org/10.1021/jf00048a059.
[19] M. Funes, M.F. Garro, R.D. Tosso, A.O. Maria, J.R. Saad, R.D. Enriz, Antinociceptive effect of *neo*-clerodane diterpenes obtained from *Baccharis Flabellata*, Fitoterapia 130 (2018) 94–99, https://doi.org/10.1016/j.fitote.2018.08.017.
[20] Z. Feng, J. Cao, Q. Zhang, L. Lin, The drug likeness analysis of anti-infammatory clerodane diterpenoids, Chin. Med. 15 (2020) 1–13, https://doi.org/10.1186/s13020-020-00407-w.
[21] Disposition No. 6344/96, Published in the Official Bulletin of the Nation No. 28567, 1st. Section January 20, 1997, Buenos Aires, Argentina. (ANMAT), 1996.
[22] N.B. Eddy, D. Leimbach, Synthetic analgesics. II. Dithienylbutenyl- and dithienylbutylamines, JPET. 107 (1953) 385–393.
[23] G. Woolfe, A.D. MacDonald, The evaluation of the analgesic action of pethidine hydrochloride, J. Pharmacol. Exp. Ther. 80 (1944) 300–307.
[24] A.P. Riley, C.E. Groer, D. Young, A.W. Ewald, B.M. Kivell, T.E. Prisinzano, J. Med. Chem. 57 (2014) 10464–10475, https://doi.org/10.1021/jm501521d.
[25] H. Wu, D. Wacker, M. Mileni, V. Katritch, G.W. Han, E. Vardy, W. Liu, A. A. Thompson, X.P. Huang, F.I. Carroll, S.W. Mascarella, R.B. Westkaemper, P. D. Mosier, B.L. Roth, V. Cherezov, R.C. Stevens, Structure of the human kappa opioid receptor in complex with JDTic, Nature 485 (2012) 327–332, https://doi.org/10.1038/nature10939.
[26] A. Sali, T.L. Blundell, Comparative protein modeling by satisfaction of spatial restraints, J. Mol. Biol. 234 (1993) 779–815, https://doi.org/10.1006/jmbi.1993.1626.
[27] O. Trott, A.J. Olson, AutoDock Vina: improving the speed and accuracy of docking with a new scoring function, efficient optimization, and multithreading, J. Comput. Chem. 31 (2010) 455–461, https://doi.org/10.1002/jcc.21334.
[28] G.M. Morris, R. Huey, W. Lindstrom, M.F. Sanner, R.K. Belew, D.S. Goodsell, A. J. Olson, AutoDock4 and AutoDockTools4: automated docking with selective receptor flexibility, J. Comput. Chem. 30 (2009) 2785–2791, https://doi.org/10.1002/jcc.21256.
[29] D.A. Case, D.S. Cerutti, T.E. Cheatham III, T.A. Darden, R.E. Duke, T.J. Giese, H. Gohlke, A.W. Goetz, D. Greene, N. Homeyer, S. Izadi, A. Kovalenko, T.S. Lee, S. LeGrand, P. Li, C. Lin, J. Liu, T. Luchko, R. Luo, D. Mermelstein, K.M. Merz, G. Monard, H. Nguyen, I. Omelyan, A. Onufriev, F. Pan, R. Qi, D.R. Roe, A. Roitberg, C. Sagui, C.L. Simmerling, W.M. Botello-Smith, J. Swails, R.C. Walker, J. Wang, R.M. Wolf, X. Wu, L. Xiao, D.M. York, P.A. Kollman, AMBER 2017, University of California, San Francisco, 2017.
[30] W. Jorgensen, J. Chandrasekhar, J. Madura, R. Impey, M. Klein, Comparison of simple potential functions for simulating liquid water, J. Chem. Phys. 79 (1983) 926–935, https://doi.org/10.1063/1.445869.
[31] K. Lindorff-Larsen, S. Piana, K. Palmo, P. Maragakis, J.L. Klepeis, R.O. Dror, D. E. Shaw, Proteins 2010 (1950) 78.
[32] J. Wang, R.M. Wolf, J.W. Caldwell, P.A. Kollman, D.A. Case, J. Comput. Chem. 25 (2004) 1157.
[33] T. Darden, D. York, L. Pedersen, Particle mesh Ewald - an N.log(n) method for Ewald sums in large systems, J. Chem. Phys. 98 (1993) 10089–10092, https://doi.org/10.1063/1.464397.
[34] S. Miyamoto, P. Kollman, Settle An analytical version of the SHAKE and RATTLE algorithm for rigid water models, J. Comput. Chem. 13 (1992) 952–962, https://doi.org/10.1002/jcc.540130805.
[35] D.R. Roe, T.E. 3rd Cheatham, PTRAJ and CPPTRAJ: software for processing and analysis of molecular dynamics trajectory data, J. Chem. Theory Compu. 9 (2013) 3084–3095, https://doi.org/10.1021/ct400341p.
[36] E.F. Pettersen, T.D. Goddard, C.C. Huang, G.S. Couch, D.M. Greenblatt, E.C. Meng, T.E. Ferrin, UCSF chimera–a visualization system for exploratory research and

analysis, J. Comput. Chem. 25 (2004) 1605–1612, https://doi.org/10.1002/jcc.20084.
[37] B.R. Miller, T.D. McGee, J.M. Swails, N. Homeyer, H. Gohlke, A.E. Roitberg, MMPBSA.Py: an efficient program for end-state free energy calculations, Theory. Comp. 8 (2012) 3314–3321, https://doi.org/10.1021/ct300418h.
[38] T. Hou, N. Li, Y. Li, W. Wang, Characterization of domain-peptide interaction interface: prediction of SH3 domain-mediated protein-protein interaction network in yeast by generic structure-based models, J. Proteome Res. 11 (2012) 2982–2995, https://doi.org/10.1021/pr3000688.
[39] N.D. Machado, O.F. Silva, R.H. de Rossi, M.A. Fernández, Cyclodextrin modified niosomes to encapsulate hydrophilic compounds, RSC Adv. 52 (2018) 29909–29916, https://doi.org/10.1039/C8RA05021J.
[40] N.D. Machado, M.A. Fernández, M. Häering, C. Saldías, D. Díaz Díaz, Niosomes encapsulated in biohydrogels for tunable delivery of phytoalexin resveratrol, RSC Adv. 9 (2019) 7601–7609, https://doi.org/10.1039/C8RA09655D.
[41] S. Elmariah, S. Chisolm, T. Sciascia, S.G. Kwatra, Modulation of the kappa and mu opioid axis for the treatment of chronic pruritus: a review of basic science and clinical implications, JAAD 7 (2022) 156–163, https://doi.org/10.1016/j.jdin.2022.03.007.
[42] A. Yilmaz, R.S. Crowley, A.M. Sherwood, T.E. Prisinzano, Semisynthesis and kappa-opioid receptor activity of derivatives of Columbin, a Furanolactone Diterpene, J. Nat. Prod. 80 (2017) 2094–2100, https://doi.org/10.1021/acs.jnatprod.7b00327.
[43] D.F. Veber, S.R. Johnson, H.Y. Cheng, B.R. Smith, K.W. Ward, K.D. Kopple, Molecular properties that influence the oral bioavailability of drug candidates, J. Med. Chem. 45 (2002) 2615–2623, https://doi.org/10.1021/jm020017n.
[44] T.L.S. Lapenda, W.A. Morais, F.J.F. Almeida, M.S. Ferraz, M.C.B. Lira, N.P. S. Santos, M.A.M. MacIel, N.S. Santos-Magalhães, Encapsulation of trans-dehydrocrotonin in liposomes: an enhancement of the antitumor activity, J. Biomed. Nanotech. 9 (2013) 499–510, https://doi.org/10.1166/jbn.2013.1554.
[45] E. Planas, S. Sánchez, L. Rodriguez, O. Pol, M.M. Puig, Antinociceptive/anti-edema effects of liposomal morphine during acute inflammation of the rat paw, Pharmacology 60 (2000) 121–127, https://doi.org/10.1159/000028356.
[46] V. Gómez-Murcia, B.R. Do Couto, J.C. Gómez-Fernández, M.V. Milanés, M. L. Laorden, P. Almela, Liposome-encapsulated morphine affords a prolonged analgesia while facilitating the extinction of reward and aversive memories, Front. Pharmacol. 10 (2019) 1–15, https://doi.org/10.3389/fphar.2019.01082.
[47] N. Mennini, P. Mura, C. Nativi, B. Richichi, L. Di Cesare Mannelli, C. Ghelardini, Injectable liposomal formulations of opiorphin as a new therapeutic strategy in pain management, Futur. Sci. OA 1 (2015) 1–10, https://doi.org/10.4155/fso.14.3.
[48] F. Rinaldi, E. Del Favero, V. Rondelli, S. Pieretti, A. Bogni, J. Ponti, F. Rossi, L. Di Marzio, D. Paolino, C. Marianecci, pH-sensitive niosomes: effects on cytotoxicity and inflammation and pain in murine models, J. Enzyme Inhib. Med. Chem. 32 (2017) 538–546, https://doi.org/10.1080/14756366.2016.1268607.
[49] C. Marianecci, S. Petralito, F. Rinaldi, P.N. Hanieh, M. Carafa, Some recent advances on liposomal and niosomal vesicular carriers, J. Drug Deliv. Sci. Technol. 32 (2016) 256–269, https://doi.org/10.1016/j.jddst.2015.10.008.
[50] C. Mircioiu, V. Voicu, V. Anuta, A. Tudose, C. Celia, D. Paolino, M. Fresta, R. Sandulovici, I. Mircioiu, Mathematical modeling of release kinetics from supramolecular drug delivery systems, Pharmaceutics 11 (2019) 1–45, https://doi.org/10.3390/pharmaceutics11030140.
[51] M.L. Bruschi, Mathematical models of drug release, in: M.L. Bruschi (Ed.), Strategies to Modify the Drug Release from Pharmaceutical Systems, Woodhead Publishing, 2015, pp. 63–86. ISBN 9780081000922.